Regeneration of Gold Surfaces Covered by Adsorbed Thiols and Proteins Using Liquid-Phase Hydrogen Peroxide-Mediated UV-Photooxidation

ARTICLE *in* THE JOURNAL OF PHYSICAL CHEMISTRY C · JANUARY 2013

Impact Factor: 4.77 · DOI: 10.1021/jp307983e

2 AUTHORS:

Blake N. Johnson
Virginia Polytechnic Institute and State Univer…
21 PUBLICATIONS **194** CITATIONS
SEE PROFILE

Raj Mutharasan
Drexel University
169 PUBLICATIONS **3,291** CITATIONS
SEE PROFILE

THE JOURNAL OF PHYSICAL CHEMISTRY C

Article

pubs.acs.org/JPCC

Regeneration of Gold Surfaces Covered by Adsorbed Thiols and Proteins Using Liquid-Phase Hydrogen Peroxide-Mediated UV-Photooxidation

Blake N. Johnson and Raj Mutharasan*

Department of Chemical and Biological Engineering, Drexel University, Philadelphia, Pennsylvania 19104, United States

Supporting Information

ABSTRACT: Quartz crystal microbalance (QCM) response of 6-mercapto-1-hexanol chemisorption was used as a model system for examining regeneration of gold (Au) surfaces covered by sulfur-based self-assembled monolayers (SAMs) using a liquid-phase UV-photooxidation (liquid-UVPO) technique. The treatment facilitated oxidation of the Au–thiolate bond in liquid as supported by time-of-flight matrix-free laser desorption/ionization mass spectrometry (LDI-TOF-MS) and post-treatment SAM reformation. The liquid-UVPO technique also showed the ability to regenerate Au surfaces covered by adsorbed proteins, demonstrated using bovine serum albumin (BSA). Comparison with Au regeneration achieved using standard piranha treatment showed the liquid-UVPO technique better preserved the original Au film properties than did piranha treatment. Piranha treatment was found to affect both surface morphology, in terms of surface roughness increase, and film crystal structure, in terms of Au ⟨111⟩ phase fractional decrease, that were relatively absent in the liquid-UVPO treatment based on atomic force microscopy (AFM) and X-ray diffraction (XRD) studies, respectively. This work gives a new liquid-phase technique for regenerating SAM- and protein-covered Au surfaces in liquid that better preserves the original properties of the Au film than standard piranha treatment. Thus, it has potential to improve measurement repeatability in sensing applications, which require Au surface regeneration.

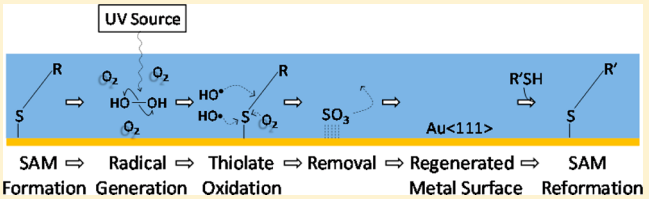

1. INTRODUCTION

Gold (Au) surfaces are used in a variety of applications including sensing, drug delivery, and catalysis. Such applications often involve initial immobilization of molecules on the Au surface to facilitate subsequent binding reactions (e.g., antibody–antigen or DNA probe-gene binding). Therefore, it is important to understand factors that affect stability of Au thin film properties, as variations in film properties will affect repeatability of resulting molecular architecture. Inherent difficulty arises due to the fact that reproducibility of surface properties can widely vary depending on the deposition technique used.[1,2] Another major source of variation in many Au-based sensing applications arises due to required cleaning and preparation of the Au surface. Thus, to achieve reproducibility in Au surface-based applications, it is critical to have techniques for regenerating Au surfaces that preserve the initial Au film, as well as to understand the effects chemical treatment can have on Au properties (e.g., morphology and crystal structure).

The Au–thiolate bond is commonly used to facilitate molecular immobilization due to its high binding strength.[1,3−6] However, its resilience also presents difficulties for Au surface regeneration, because removing adsorbed thiols is not trivial due to the requirement of breaking the stable Au–thiolate bond.[1,7] Thus, as cleaning and regenerating Au is essential, various techniques for regenerating Au have been reported. Traditional wet-chemistry techniques include hydrogen peroxide (H_2O_2)–sulfuric acid solutions (known as piranha solution),[1] H_2O_2–ammonium hydroxide solutions,[8] sodium borohydride solutions,[9] sulfochromic acid,[10] and nitric acid–hydrochloric acid solutions (known as aqua regia).[11] However, they are relatively aggressive and have been shown to alter Au surface structure, damage sensor-associated components that are mechanically coupled to Au, adversely affect monolayer properties, and form Au oxides.[10,12,13] Electrochemical techniques have also been used in liquid environments, but they require integration into an electrochemical cell.[14] Gas-phase techniques, such as reactive plasma,[15,16] UV-photooxidation (UVPO),[16,17] ozonolysis,[18,19] and thermal desorption,[20] have also been investigated. However, they are not suitable for in situ liquid-based applications and increase the likelihood of sensor contamination when carried out ex situ. The most commonly used technique for regenerating Au has been piranha treatment; however, its effects on Au film properties have been only minimally investigated.

A liquid-phase UVPO-based technique for removing the Au–thiolate bond presents an attractive alternative because the experimental setup is relatively straightforward, requiring only a UV-source and radical-generating reagent.[21] It would also be less aggressive relative to other wet-chemistry techniques

Received: August 10, 2012
Revised: December 8, 2012
Published: December 27, 2012

   dx.doi.org/10.1021/jp307983e | J. Phys. Chem. C 2013, 117, 1335−1341

because the concentration of radical-forming species, the UV radiation input, and the pH could be optimized to avoid excessive reactivity. However, UVPO of thiols on Au has only been carried out in the gas phase[16−19,22−28] due to ease of design and challenge of reduced radical-forming species levels in liquid, a limitation that we overcome in this Article. One study has suggested that UV-induced oxidation of the Au−thiolate indeed occurs in liquid,[29] but did not extend the idea to development of a new technique for removing immobilized thiol molecules. In this Article, we present a liquid-based hydrogen peroxide (H_2O_2)-mediated UV-photooxidation (liquid-UVPO) technique for removing chemisorbed thiols and immobilized proteins from gold (Au) surfaces that better preserves the original Au surface properties relative to piranha treatment. The technique was validated using two commonly immobilized reagents in liquid sensing applications, 6-mercapto-1-hexanol (MCH) and bovine serum albumin (BSA), by quartz crystal microbalance (QCM), time-of-flight matrix-free laser desorption/ionization mass spectrometry (LDI-TOF-MS), atomic force microscopy (AFM), and X-ray diffraction (XRD) studies.

2. EXPERIMENTAL SECTION

2.1. Materials. Concentrated sulfuric acid, hydrogen peroxide (30% w/w, H_2O_2), and sodium hydroxide were purchased from Fisher. Thiol compound 6-mercapto-1-hexanol (MCH) and bovine serum albumin (BSA) were from Fluka and Sigma-Aldrich, respectively. Ethanol (EtOH, 200 proof, Decon Laboratories, Inc.) and deionized (DI) water (18 MΩ) were used in all sample preparation and rinsing procedures. Sodium hydroxide (NaOH, Fisher) was used for adjusting H_2O_2 solution pH. Poly(ethylene glycol) (PEG, 600, 1000, and 1500 average molecular weight) standards, sodium bromide (NaBr), HPLC-grade acetonitrile (AN), trifluoroacetic acid (TFA), and α-cyano-4-hydroxycinnamic acid 99% (CHCA) were from Sigma-Aldrich.

2.2. Quartz Crystal Microbalance (QCM). A commercially available gold (Au)-coated QCM and flow cell (Stanford Research Systems, Inc. QCM model 200, Sunnyvale, CA) were used in all experiments. Prior to a binding experiment, the Au surface was cleaned by either oxygen (O_2) plasma for 20 min (Harrick Plasma, Ithica, NY, model PDC-001), freshly prepared piranha solution (3:1 concentrated sulfuric acid:30% H_2O_2) for 5 min, or liquid-UVPO for 90 min. Caution: Piranha solution is highly corrosive and should be handled with care. The surface was subsequently rinsed with copious EtOH and DI water, and finally blown dry with nitrogen.

2.3. UV-Treatment. A commercially available mercury lamp (UVP, LLC, model OG-1, Upland, CA) emitting maximum shortwave UV radiation bands at 185 and 254 nm was used as the UV-source for all experiments. Minimum 254 nm irradiance was 3.2 mW/cm^2 at 1 in. distance.

2.4. Time-of-Flight Matrix-Free Laser Desorption/Ionization Mass Spectrometry (LDI-TOF-MS). A commercially available Autoflex III Smartbeam MALDI-TOF mass spectrometer (Bruker Daltonics) was used for all mass spectrometry analyses (detailed information is given in section S.1 of the Supporting Information).

2.5. X-ray Diffraction (XRD). XRD measurements in the Bragg−Brentano geometry were performed on a commercially available system (Rigaku, Smartlab) using Cu K_α radiation. Spectra were recorded at 40 kV and 30 mA with a step size of 0.1° (2θ). Au substrates analyzed were prepared by sputtering Au at 100 nm thick (Denton Vacuum LLC, Moorestown, NJ) onto already gold-coated silicon wafers (Sigma-Aldrich), exposure to thiol solution for 30 min, and Au regeneration by either piranha- or liquid-UVPO treatment. Associated statistics were obtained as average signal over three simultaneously treated samples. Variance in repeated measurement was ±2%.

2.6. Atomic Force Microscopy (AFM). Contact-mode AFM measurements were preformed on a commercially available Nanoscope III Multiprobe scanning probe microscope (Digital Instruments) to examine the effects of piranha- and liquid-UVPO treatment on Au surface morphology. Non-conductive silicon nitride AFM probes were used (Veeco, model DNP-S10). AFM micrographs over a 1.25 × 1.25 μm^2 area were obtained at a scan rate of 1 Hz. Au substrates analyzed were prepared identically to those analyzed by XRD. Surface root-mean-square (RMS) roughness values and line profiles were obtaining using vendor-provided software.

3. RESULTS AND DISCUSSION

3.1. Typical Experiment. QCM has been used extensively as a technique for measuring binding between molecules and surfaces as the resonant frequency response is directly related to change in surface mass density.[30] For a typical binding experiment, the freshly cleaned QCM crystal was installed in the flow cell, flowing DI water was established at 80 μL/min (23 °C), and the crystal resonant frequency was allowed to reach a constant value. Subsequently, the flow was switched to a 65 μM aqueous MCH solution without flow interruption. As shown in Figure 1A, over the next 25 min resonant frequency decreased exponentially due to MCH chemisorption on Au. The formation of thiolates on gold (RS−Au) due to chemisorption of thiol molecules (RSH) can be described by the following reaction, which remains a focus of research to date:[31]

$$\mathrm{RSH} + \mathrm{Au} \rightarrow \mathrm{RS{-}Au} + \frac{1}{2}\mathrm{H_2} \quad (1)$$

Once binding equilibrium was reached, the flow was switched back to DI water, which caused no further change in resonant frequency indicating that there were no observable density or viscosity effects, and thus the net resonant frequency shift was attributable to added mass of chemisorbed MCH. As shown in Figure 1A, mass spectra of the surface prior to- and post-MCH exposure also support the claim that sensor response correlates with thiol chemisorption. Ultimately, the binding caused a net shift of −13.3 ± 3.6 Hz (n = 2), which compares reasonably with the expected value (−5.3 Hz) and had a binding rate constant (k_{obs}) of 0.11 min^{-1} based on data in the initial rate period (see Figure 1B; supporting calculations given in section S.2 of the Supporting Information). We note that this response serves as a reference for analysis of the liquid-UVPO technique.

3.2. Driving Force Behind Liquid-Phase UV-Photooxidation (liquid-UVPO). The difficulty of regenerating Au surfaces covered by thiol-based self-assembled monolayers (SAMs) arises from the considerable binding energy of the Au−thiolate species (RS−Au), which makes it difficult to remove unless the bond is oxidized. This makes use of hydroxyl radicals attractive. An aqueous hydrogen peroxide (H_2O_2) solution exposed to UV radiation ($h\nu$) will undergo UV-photolysis by:[21]

dx.doi.org/10.1021/jp307983e | J. Phys. Chem. C 2013, 117, 1335−1341

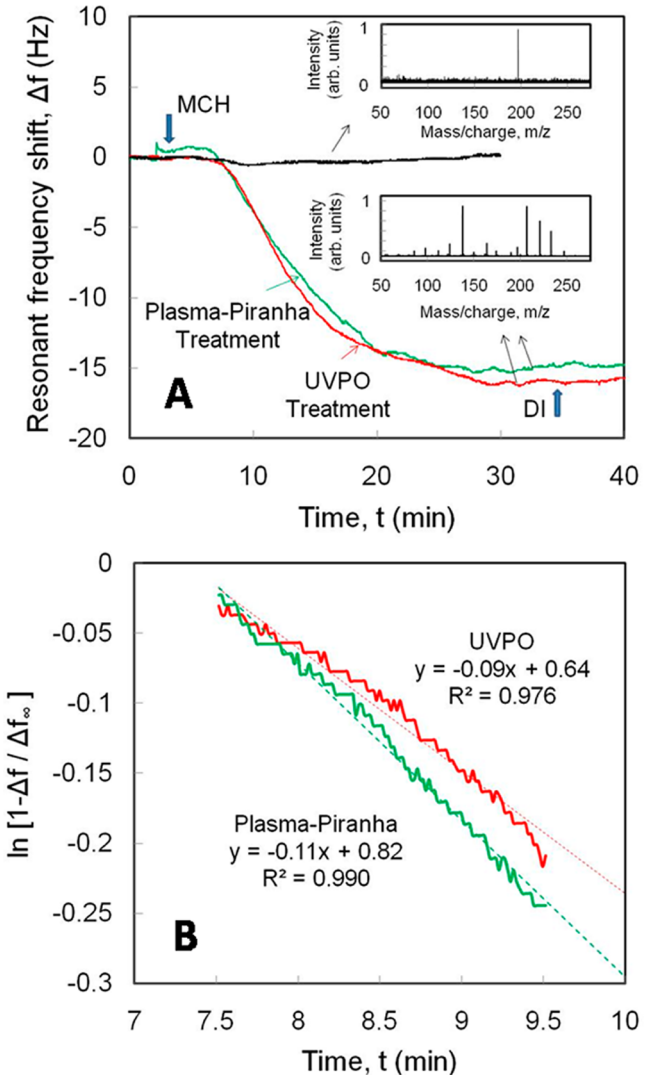

Figure 1. (A) Typical MCH binding response measured post-plasma-piranha treatment as compared to MCH binding response post-liquid-UVPO treatment and a control showing sensor response in the absence of thiol. Insets show mass spectra of the freshly deposited Au versus Au covered by adsorbed MCH. (B) Kinetic analysis of responses shown in (A) by Langmuir kinetics gives observable rate constants (k_{obs}) for plasma-piranha- and liquid-UVPO treatment of 0.11 and 0.09 min^{-1}, respectively.

$$\frac{1}{2}H_2O_2 + h\nu \rightarrow OH^{\bullet} \quad (2)$$

generating two hydroxyl radicals ($OH^{\bullet}$) from one molecule of H_2O_2. Enhancing dissolved oxygen (DO) in the solvent also produces oxygen, superoxide, and hydroperoxyl radicals.[21] These reactive radical species then oxidize thiolate species to sulfur oxides, which have low affinity for Au and can be readily removed by rinsing with polar solvents to regenerate the Au surface (see Figure S.2 of the Supporting Information).[1] The complete reaction scheme is given as:

$$RSH + Au \rightarrow RS{-}Au + \frac{1}{2}H_2 \quad (3)$$

$$\frac{1}{2}H_2O_2 + h\nu \rightarrow HO^{\bullet} \quad (4)$$

$$RS{-}Au + O_2 + HO^{\bullet} \rightarrow RSO_3H + Au \quad (5)$$

which yields the following net reaction:

$$RSH + \frac{1}{2}H_2O_2 + O_2 + h\nu \rightarrow RSO_3H + \frac{1}{2}H_2 \quad (6)$$

It is possible to calculate the thermodynamic driving force of the net reaction using available thermodynamic information.[32,33] Table 1 lists the corresponding heats of formation

Table 1. Summary of Thermodynamic Parameters for the Liquid-UVPO Technique Based on Reaction Scheme Presented in Equations 3–6[a]

species	stoichiometric coefficient, ν_i	heat of formation, ΔH°_f (kcal/mol)	standard molar entropy, ΔS°_f (cal/(mol·K))	free energy of formation, ΔG°_f (kcal/mol)
RSH	−1.0	−11.2	39.0	−22.8
H_2O_2	−0.5	−31.8	55.8	−48.4
O_2	−1.0	0.0	0.0	0.0
H_2	0.5	0.0	0.0	0.0
RSO_3H	1.0	−178.1	74.0	−200.2
net reaction		−151.0	7.1	−153.2

[a]A methyl group was selected as R to provide a basis due to availability of thermodynamic data.[32,33]

(ΔH_f°), standard molar entropy (ΔS_f°), and free energy of formation (ΔG_f°) for each species (i) and the net reaction (eq 6) calculated as:

$$\Delta H^{\circ} = \sum_{i=1}^{n} \nu_i \Delta H_{f,i}^{\circ} \quad (7)$$

$$\Delta S^{\circ} = \sum_{i=1}^{n} \nu_i \Delta S_{f,i}^{\circ} \quad (8)$$

$$\Delta G^{\circ} = \Delta H^{\circ} - T\Delta S^{\circ} \quad (9)$$

As shown in Table 1, the net reaction is thermodynamically favorable as indicated by associated $\Delta G^{\circ} = -153.2$ kcal/mol. We note that specific heat and heat of mixing effects were ignored in these calculations.

To increase the reaction rate, it is also useful to have H_2O_2 and DO present in excess to the total number of Au−thiolate species. Therefore, an O_2-saturated 12.5% w/w H_2O_2 solution was used (pH = 8.0, adjusted using NaOH) because the 400 μL sample volume contained 1.5 mmol of radical species, which is far greater than the ∼0.8 nmol of chemisorbed thiol present on the 113 mm^2 area. We also note that it was not the objective of the current work to optimize the H_2O_2 concentration, but only to choose a concentration that would facilitate complete oxidation of Au−thiolate species. Further, because water absorbs infrared radiation (IR), the aqueous solution also acts as an IR-filter removing any IR-associated lamp effects.

3.3. Liquid-UVPO Surface Regeneration. Having established that an MCH layer has been chemisorbed on Au, and the experimental design provides suitable levels of radical-forming reagent to facilitate thiol removal, we next determined if liquid-UVPO treatment could remove the chemisorbed thiol. Therefore, after the MCH was chemisorbed in a flow-format, the Au surface was rinsed with copious amounts of EtOH and DI water to remove any residual or loosely bound thiol. In preparation for liquid-UVPO treatment, the QCM crystal was

dx.doi.org/10.1021/jp307983e | J. Phys. Chem. C 2013, 117, 1335−1341

immersed in 400 μL of O_2-saturated aqueous H_2O_2 solution, and the UV-source was placed 1 cm directly above the liquid surface creating an effective path length of ~1.2 cm (0.2 cm liquid and 1.0 cm air, see Figure S.2 of the Supporting Information). The UV-source was then turned on to begin treatment. The resulting response over a 90 min period (Figure 2A) showed initial rapid resonant frequency increase followed by a slower rise, giving an overall response of ~150 Hz. During the remainder of the UV-on period, the resonant frequency remained relatively constant but with an increased noise level. We attribute this dynamic response to a combination of effects, which include oxidation of the Au–thiolate bond (see mass spectra verification shown in Figure 2A and section S.3 of the Supporting Information), UV-acoustic wave coupling,[29] UV-induced radical formation in the bulk liquid,[21] evolution of DO, and small temperature increases (Figure 2B). Ultimately, when the UV-source was turned off, the resonant frequency decreased to a value slightly above the initial resonant frequency prior to UV-exposure (~50 Hz). Comparison of mass spectra shown in Figures 1A and 2A showed the liquid-UVPO treatment caused changes in the SAM consistent with oxidation (see section S.1 of the Supporting Information for further discussion). The net resonant frequency shift caused by the UV-treatment can be attributed to oxidation of the Au–thiolate bond, changes in liquid density or viscosity caused by radical formation, and small temperature increase. To ensure hydroxyl radical concentration remained high, the H_2O_2 solution was replaced every 30 min. We also note that significant noise present in the resonant frequency response was caused by degassing of the O_2-saturated H_2O_2 solution and was absent when using an unsaturated solution. A control experiment in which the Au surface was masked from UV-exposure caused no change in resonant frequency over the same time period, indicating that the UV radiation played a critical role in initiating the oxidation reaction. This suggests removal of thiolate species is not simply due to proton storage of H_2O_2, which causes thiolate desorption by Le Chatelier's principle.

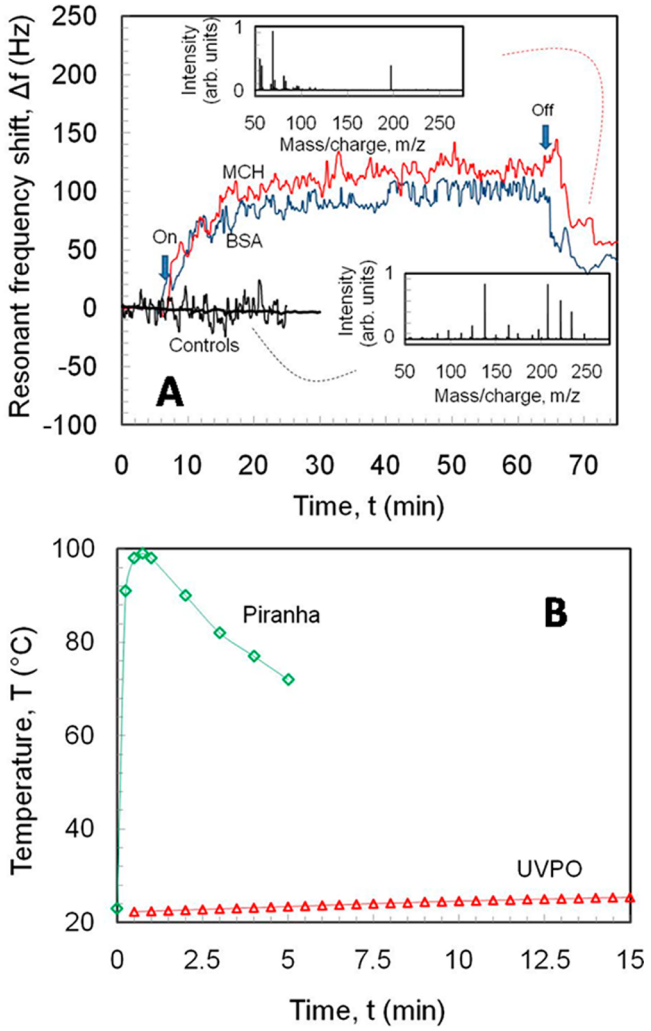

Figure 2. (A) QCM resonant frequency response during liquid-UVPO treatment of both thiol- and protein-covered Au surfaces. Arrows show times at which UV-source was turned on and off. The UV-exposure period gave a net increase in QCM resonant frequency in both cases, while in the absence of UV, the QCM resonant frequency remained constant. Increased noise level was due to evolution of DO from the O_2-saturated H_2O_2 solution, which was significantly reduced in the absence of DO. Mass spectra insets show the treatment's oxidizing effect on the SAM. (B) Treatment-dependent temperature profiles for piranha- and liquid-UVPO treatments.

3.4. Chemisorption Post Liquid-UVPO Treatment. After the liquid-UVPO treatment, we tested if, and to what extent, the chemisorbed thiol had been removed from the Au surface. The Au surface was first rinsed with polar solvents EtOH and DI water to remove products of the UVPO reaction (oxidized sulfur and organic fragments) and expose the regenerated Au ⟨111⟩ sites.[1] Rinsing was carried out for 2 min alternating between EtOH and DI water. After being rinsed, the QCM was blown dry with nitrogen, installed in the flow cell, and allowed to stabilize under the same conditions used during the initial MCH chemisorption. Once again, after the resonant frequency stabilized in flowing DI water, the flow was changed to the same MCH solution as used initially. As previously observed, the resonant frequency decreased in a similar fashion due to chemisorption, and ultimately gave a net shift of -13.6 ± 4.3 Hz ($n = 2$) after rinse with DI water (Figure 1A). The ratio of frequency shift that occurred on the plasma-piranha-cleaned surface to the frequency shift that occurred on the liquid-UVPO-treated surface gives a quantitative measure of the percentage of the overall Au–thiolate bond removal. On the basis of the responses, we conclude that $99 \pm 5\%$ ($n = 3$) of the original monolayer was removed using the liquid-UVPO technique. We also note that in the absence of UV, re-exposure of Au to MCH caused no net shift in the resonant frequency, indicating that MCH does not spontaneously desorb or become removed by only rinsing with polar solvent. As was done previously, the initial kinetics were analyzed using a first-order Langmuir kinetics rate model,[12] which gave a rate constant of 0.09 min^{-1}, comparable to that obtained on the initial surface (see Figure 1B). The close agreement in k_{obs} and net resonant frequency shift both prior to- and post-treatment suggests that the liquid-UVPO technique completely regenerated the Au and did not adversely influence binding kinetics or fractional coverage. Similarly, as shown in Figure 3, we also found the liquid-UVPO technique was capable of removing adsorbed bovine serum albumin from the Au surface comparable with piranha- and plasma treatment (details given in section S.4 of the Supporting Information). An excellent discussion of potential removal mechanisms for proteins can be found elsewhere.[34]

dx.doi.org/10.1021/jp307983e | J. Phys. Chem. C 2013, 117, 1335–1341

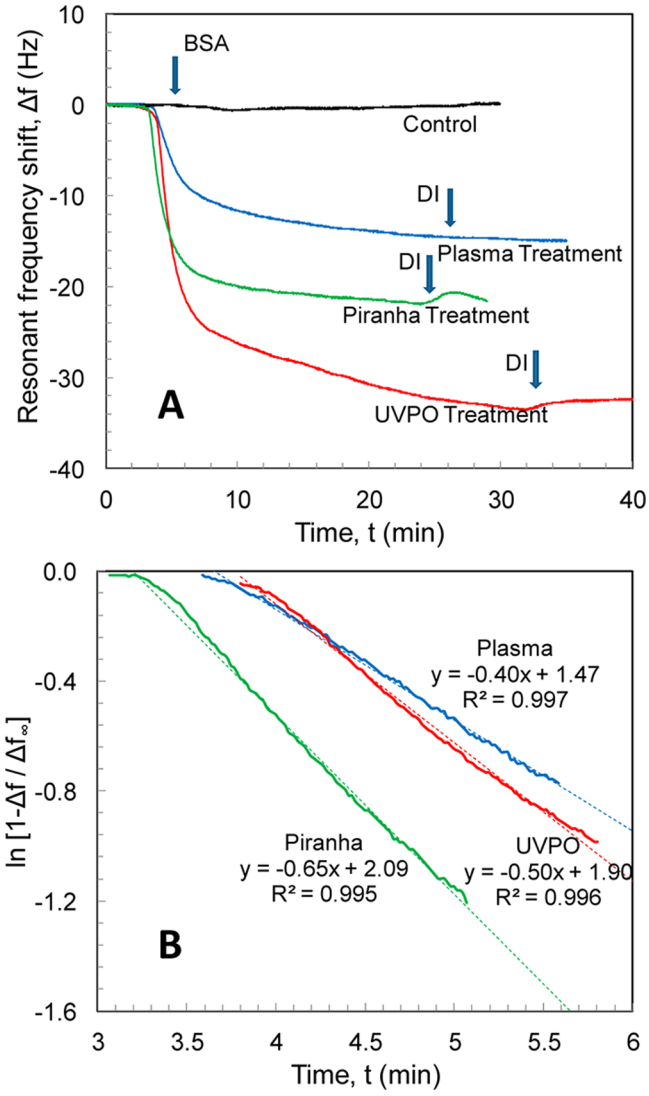

Figure 3. (A) Typical BSA binding response corresponding to a surface regenerated by 20 min O_2-plasma treatment or 5 min of piranha treatment as compared to response measured post-liquid-UVPO. (B) Kinetic analysis of responses shown in (A) by Langmuir kinetics gives observable rate constants (k_{obs}) of plasma-, piranha-, and liquid-UVPO-treated Au surfaces of 0.40, 0.65, and 0.50 min^{-1}, respectively.

3.5. Investigation of Treatment Effects on Au Surface Microstructure and Crystal Structure. Given that the liquid-UVPO technique showed the ability to regenerate Au surfaces at levels comparable with piranha treatment, it was of interest to compare their effects on surface microstructure. Thus, the liquid-UVPO technique was analyzed in reference to both a freshly deposited Au sample and a piranha-treated sample. Figure 4A–C shows the AFM micrographs of freshly deposited Au, Au regenerated using piranha treatment, and Au regenerated using liquid-UVPO treatment, respectively. The piranha treatment caused the greatest change in the Au microstructure, while liquid-UVPO treatment caused only minor changes. For example, the RMS roughness values of the freshly deposited Au, piranha-treated Au, and the liquid-UVPO-treated Au were 6.5, 13.1, and 11.6 nm, respectively. Significant pitting defects and height variations in Au were also caused by piranha treatment. These features were absent in both the liquid-UVPO-treated Au and the freshly deposited Au.

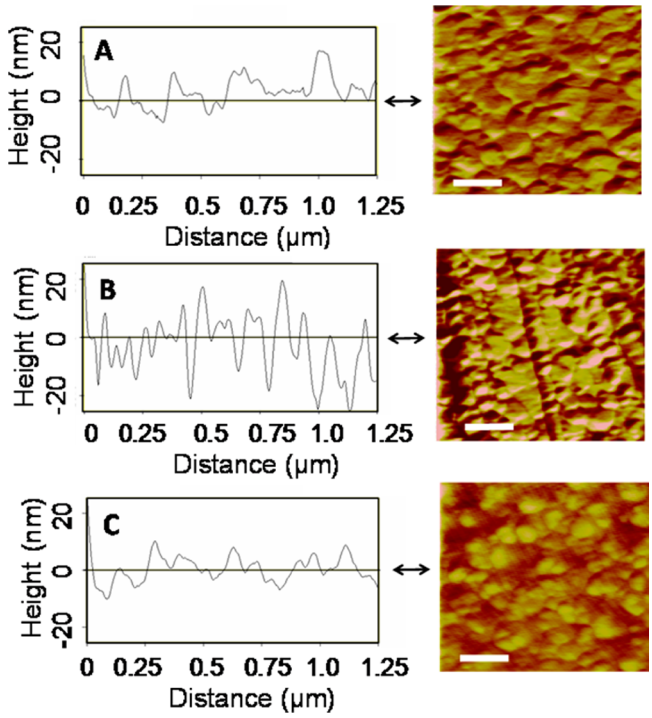

Figure 4. AFM micrographs of freshly deposited Au (A), Au post-piranha treatment (B), and Au post-liquid-UVPO treatment (C). Corresponding 2D line-analyses of substrate height shows the variance in sample height. Scale bar corresponds to 250 nm. Height scale ranges between 0 and 50 nm.

Another study observed similar damaging effects of piranha treatment, which involved delamination of the Au film from the substrate.[10] Thus, this analysis suggests that liquid-UVPO is an advantageous technique, as it better preserves the original Au surface morphology when removing bound thiol molecules.

We next investigated the effects of both treatments on Au crystal structure, as bulk thin film properties are also important in many applications. Thus, XRD measurements were also carried out. Figure 5A shows XRD spectra over the 30–90° 2θ-range. Three peaks were observed in the control Au sample at 2θ values of 38.2°, 44.6°, and 81.7°, which corresponds to Au ⟨111⟩, Au ⟨200⟩, and Au ⟨222⟩ planes, respectively.[35] Comparison of XRD spectra from piranha-treated and liquid-UVPO-treated Au with the spectra from the freshly deposited Au revealed piranha treatment also caused recrystallization effects that were less pronounced in liquid-UVPO treatment. Figure 5B shows the analysis of the XRD spectra in terms of the percent crystallinity of each phase. The freshly deposited Au was 85.1% Au ⟨111⟩, 2.4% Au ⟨200⟩, and 12.5% Au ⟨222⟩. Analysis of the piranha-treated sample showed piranha-treatment caused the Au ⟨111⟩ phase to decrease by 13.0%, and the Au ⟨200⟩ and Au ⟨222⟩ phases to increase by 6.0% and 6.9%, respectively. We note that such a decrease in the Au ⟨111⟩ phase caused by piranha treatment is of importance, because the majority of thiol–Au-based applications are based on Au ⟨111⟩ site binding.[10] Alternatively, liquid-UVPO treatment caused essentially no change in the Au ⟨111⟩ concentration (0.4% increase) and relatively less changes in the Au ⟨200⟩ and Au ⟨222⟩ concentrations (2.9% increase and 3.3% decrease, respectively). We do note that in another study, recrystallization effects were also observed for piranha treatment of Au surfaces.[36] Thus, both AFM and XRD measure-

dx.doi.org/10.1021/jp307983e | J. Phys. Chem. C 2013, 117, 1335–1341

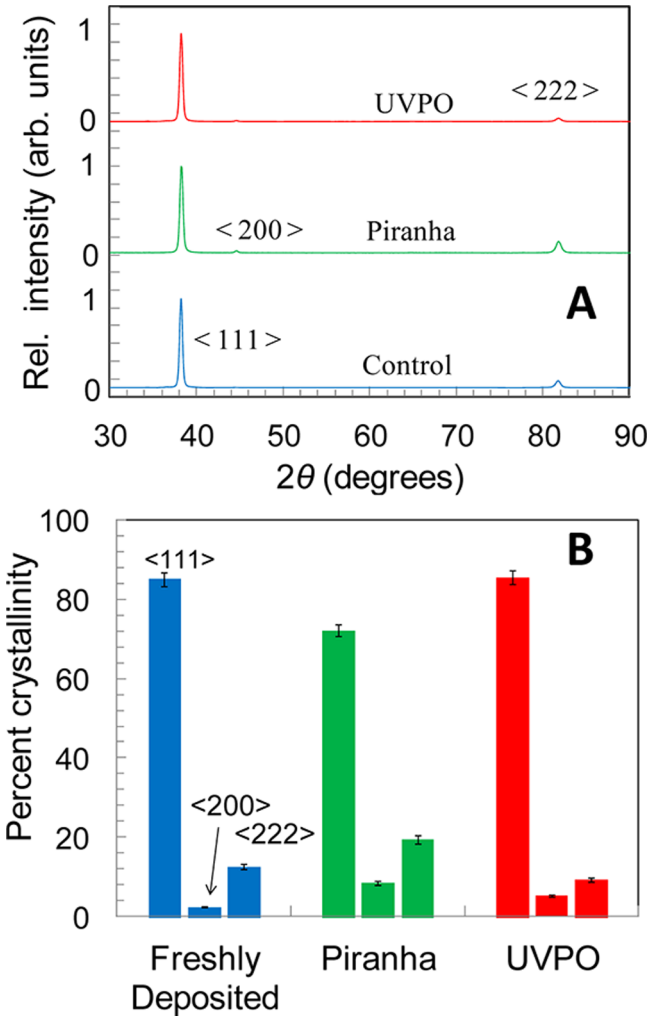

Figure 5. (A) XRD spectra of freshly deposited Au, piranha-treated Au, and liquid-UVPO-treated Au. (B) Breakdown of the percent crystallinity of multiple Au phases.

ments indicate liquid-UVPO treatment is an attractive alternative wet-chemistry treatment technique as it better maintains the properties of the initially deposited Au film in terms of both surface morphology and crystal structure.

3.6. Driving Forces Behind Treatment Effects on Au Properties. Given the different effects piranha- and liquid-UVPO treatment had on Au surface morphology and crystallinity, we examined potential driving forces behind the observed changes. As shown in Figure 2B, the associated temperature effects varied significantly in each treatment. Piranha treatment caused a maximum temperature (T_{max}) of 98 °C, while liquid-UVPO treatment caused only a small temperature increase (~3 °C). The maximum strain ($\varepsilon = \Delta L/L_0$) and strain rate ($\dot{\varepsilon}$) are given as the following, respectively:

$$\varepsilon = \alpha_L \Delta T_{max} \quad (10)$$

$$\dot{\varepsilon} = \alpha_L \frac{dT}{dt} \quad (11)$$

where α_L is the linear thermal expansion coefficient of Au ($\alpha_L = 1.4 \times 10^{-5}$ °C^{-1}).[32] Thus, piranha treatment causes a maximum strain of 1.1×10^{-3}, which corresponds to a 0.1 nm expansion in the Au. On the other hand, based on the relatively lower T_{max}, liquid-UVPO treatment causes significantly less expansion of the Au film (less than 0.01 nm), making the thermal-induced strain in the Au film during piranha treatment greater than an order of magnitude higher than during liquid-UVPO treatment. Approximating dT/dt in eq 11 with the slope of the initial rate period shown in Figure 2B ($\Delta T/\Delta t$) also shows the strain rate differs significantly, by more than 2 orders of magnitude. The significant differences arise due to the fact that T_{max} is reached in ~1 min for piranha treatment and 15 min for liquid-UVPO treatment, yielding $\Delta T/\Delta t$ = 76 and 0.2 °C/min, respectively. These large differences in associated thermal-mechanical effects suggest a thermal-mechanical driving force may be responsible for piranha treatment-induced damage, which is absent in the liquid-UVPO treatment.

It is well established that strained materials progress toward a state of minimized strain energy through relaxation processes. The experimental observations suggest two possible explanations for the observed changes in relative levels of Au phases caused by piranha treatment: (1) the Au ⟨200⟩ and Au ⟨222⟩ phases are more thermodynamically favorable at elevated temperature, which become trapped in a metastable state upon rapid cooling, or (2) the high strain rate causes rearrangement due to minimization of strain energy along grain boundaries, which decreases the Au ⟨111⟩ phase and increases the relative fraction of ⟨200⟩ and ⟨222⟩ phases present. However, the former case is less probable as the diffusion coefficient of Au atoms in the Au film is very small at 98 °C,[37] suggesting Au atoms could not significantly rearrange by diffusion during treatment over large length scales. We note that the true driving force still remains not well understood; however, various studies have also shown thermal-mechanical effects can affect thin metal film properties as we show here. For example, thermally induced strain of Au films on silicon substrates was previously shown to enable cluster formation arising from relaxation effects.[38] It was also shown that annealing of Au−lanthanum thin films at 50−80 °C followed by rapid quenching led to film recrystallization arising from thermally assisted interdiffusion among other effects.[39] Thus, while the driving force for oxidation of immobilized thiol species by liquid-UVPO treatment was minimization of chemical potential energy, the driving force for changes in Au film properties appears to be primarily through associated thermal-mechanical effects and minimization of strain energy.

4. CONCLUSION

We have shown that the liquid-phase H_2O_2-mediated UV-photooxidation technique (liquid-UVPO) is effective for completely regenerating Au surfaces covered by adsorbed thiol molecules or proteins. The technique is both suitable for subsequent in situ regeneration and maintains the original Au ⟨111⟩ site concentration. Time-of-flight matrix-free laser desorption/ionization (LDI-TOF) mass spectrometry supported the hypothesis that removal was due to treatment-induced oxidation. Atomic force microscopy (AFM) and X-ray diffraction (XRD) studies confirmed that the liquid-UVPO technique better maintained the original Au properties than did piranha treatment. Piranha treatment was observed to alter Au surface morphology and crystal structure, which may help better describe its influence on repeatability and reproducibility of measurement. This technique has the potential to contribute toward improving throughput and multiplexing capabilities of liquid flow-based sensing applications. The characterization also provides new physical insights into the effects of surface treatment on Au thin film properties.

dx.doi.org/10.1021/jp307983e | J. Phys. Chem. C 2013, 117, 1335−1341

■ ASSOCIATED CONTENT

Supporting Information

Additional information is given on mass spectrometry measurements, predicted QCM resonant frequency shifts, binding kinetics calculations, removal of adsorbed proteins from Au using liquid-UVPO, and experimental design. This material is available free of charge via the Internet at http://pubs.acs.org.

■ AUTHOR INFORMATION

Corresponding Author

*Tel.: (215) 895-2236. Fax: (215) 895-5837. E-mail: mutharasan@drexel.edu.

Notes

The authors declare no competing financial interest.

■ ACKNOWLEDGMENTS

We are grateful for the generous support of NSF Grant CBET-082987, which provided the entire funding for the reported work. We also gratefully acknowledge Dr. Timothy Wade and Prof. Kevin Owens of the Chemistry Department, Drexel University, for assistance with mass spectrometry measurements and meaningful discussions.

■ REFERENCES

(1) Love, J. C.; Estroff, L. A.; Kriebel, J. K.; Nuzzo, R. G.; Whitesides, G. M. *Chem. Rev.* **2005**, *105*, 1103−1169.
(2) Mertens, J.; Calleja, M.; Ramos, D.; Taryn, A.; Tamayo, J. *J. Appl. Phys.* **2007**, *101*, 034904.
(3) Prime, K. L.; Whitesides, G. M. *Science* **1991**, *252*, 1164−1167.
(4) Samanta, D.; Sarkar, A. *Chem. Soc. Rev.* **2011**, *40*, 2567−2592.
(5) Chaki, N. K.; Vijayamohanan, K. *Biosens. Bioelectron.* **2002**, *17*, 1−12.
(6) Wink, T.; van Zuilen, S.; Bult, A.; van Bennekom, W. *Analyst* **1997**, *122*, 43R−50R.
(7) Gronbeck, H.; Curioni, A.; Andreoni, W. *J. Am. Chem. Soc.* **2000**, *122*, 3839−3842.
(8) Kim, D. J.; Pitchimani, R.; Snow, D. E.; Hope-Weeks, L. J. *Scanning* **2008**, *30*, 118−122.
(9) Yuan, M. Q.; Zhan, S. H.; Zhou, X. D.; Liu, Y. J.; Feng, L.; Lin, Y.; Zhang, Z. L.; Hu, J. M. *Langmuir* **2008**, *24*, 8707−8710.
(10) Kang, J.; Rowntree, P. A. *Langmuir* **2006**, *23*, 509−516.
(11) Ju, H.; Leech, D. *Phys. Chem. Chem. Phys.* **1999**, *1*, 1549−1554.
(12) Karpovich, D. S.; Blanchard, G. J. *Langmuir* **1994**, *10*, 3315−3322.
(13) Ron, H.; Rubinstein, I. *Langmuir* **1994**, *10*, 4566−4573.
(14) Schneider, T. W.; Buttry, D. A. *J. Am. Chem. Soc.* **1993**, *115*, 12391−12397.
(15) Raiber, K.; Terfort, A.; Benndorf, C.; Krings, N.; Strehblow, H.-H. *Surf. Sci.* **2005**, *595*, 56−63.
(16) Huang, J. Y.; Hemminger, J. C. *J. Am. Chem. Soc.* **1993**, *115*, 3342−3343.
(17) Brewer, N. J.; Janusz, S.; Critchley, K.; Evans, S. D.; Leggett, G. J. *J. Phys. Chem. B* **2005**, *109*, 11247−11256.
(18) Norrod, K. L.; Rowlen, K. L. *J. Am. Chem. Soc.* **1998**, *120*, 2656−2657.
(19) Zhang, Y.; Terrill, R. H.; Tanzer, T. A.; Bohn, P. W. *J. Am. Chem. Soc.* **1998**, *120*, 2654−2655.
(20) Delamarche, E.; Michel, B.; Kang, H.; Gerber, C. *Langmuir* **1994**, *10*, 4103−4108.
(21) Yue, P. L. *Chem. Eng. Sci.* **1993**, *48*, 1−11.
(22) Hutt, D. A.; Leggett, G. J. *J. Phys. Chem.* **1996**, *100*, 6657−6662.
(23) Zhang, Y.; Terrill, R. H.; Bohn, P. W. *Chem. Mater.* **1999**, *11*, 2191−2198.
(24) Cooper, E.; Leggett, G. J. *Langmuir* **1998**, *14*, 4795−4801.
(25) Cooper, E.; Leggett, G. J. *Langmuir* **1999**, *15*, 1024−1032.
(26) Tam-Chang, S.-W.; Biebuyck, H. A.; Whitesides, G. M.; Jeon, N.; Nuzzo, R. G. *Langmuir* **1995**, *11*, 4371−4382.
(27) Mirsaleh-Kohan, N.; Bass, A. D.; Sanche, L. *Langmuir* **2010**, *26*, 6508−6514.
(28) Schoenfisch, M. H.; Pemberton, J. E. *J. Am. Chem. Soc.* **1998**, *120*, 4502−4513.
(29) Thompson, M.; Ellis, J. S.; Ryan, T.; Lyle, E.-L. *Anal. Lett.* **2010**, *43*, 1801−1811.
(30) Cheng, C. I.; Chang, Y. P.; Chu, Y. H. *Chem. Soc. Rev.* **2012**, *41*, 1947−1971.
(31) Vericat, C.; Vela, M. E.; Benitez, G.; Carro, P.; Salvarezza, R. C. *Chem. Soc. Rev.* **2010**, *39*, 1805−1834.
(32) *Knovel Critical Tables*, 2nd ed.; Knovel: New York, 2003.
(33) Guthrie, J. P.; Stein, A. R.; Huntington, A. P. *Can. J. Chem.* **1998**, *76*, 929−936.
(34) Norde, W. *Pure Appl. Chem.* **1994**, *66*, 491−496.
(35) Uosaki, K.; Shen, Y.; Kondo, T. *J. Phys. Chem.* **1995**, *99*, 14117−14122.
(36) Twardowski, M.; Nuzzo, R. G. *Langmuir* **2002**, *18*, 5529−5538.
(37) Mallard, W. C.; Gardner, A. B.; Bass, R. F.; Slifkin, L. M. *Phys. Rev.* **1963**, *129*, 617−625.
(38) De Los Santos, V. L.; Lee, D.; Seo, J.; Leon, F. L.; Bustamante, D. A.; Suzuki, S.; Majima, Y.; Mitrelias, T.; Ionescu, A.; Barnes, C. H. W. *Surf. Sci.* **2009**, *603*, 2978−2985.
(39) Schwarz, R. B.; Johnson, W. L. *Phys. Rev. Lett.* **1983**, *51*, 415−418.